ACS APPLIED MATERIALS & INTERFACES

Research Article

www.acsami.org

Nanoscale Damping Characteristics of Boron Nitride Nanotubes and Carbon Nanotubes Reinforced Polymer Composites

Richa Agrawal, Andy Nieto, Han Chen, Maria Mora, and Arvind Agarwal*

Nanomechanics and Nanotribology Laboratory, Department of Mechanical and Materials Engineering, Florida International University, Miami, Florida 33174, United States

ABSTRACT: This study compares the damping behavior of boron nitride nanotubes (BNNTs) and carbon nanotubes (CNTs) as reinforcement in PLC, a biodegradable copolymer. The damping behavior of PLC composites reinforced with 2 wt % or 5 wt % nanotube filler is evaluated by nanodynamic mechanical analysis (NanoDMA). The addition of 2 wt % CNT leads to the greatest enhancement in damping (tan δ) behavior. This is attributed to pullout in CNTs because of lower interfacial shear strength with the polymer matrix and a more effective sword-in-sheath mechanism as opposed to BNNTs which have bamboo-like nodes. BNNTs however have a superior distribution in the PLC polymer matrix enabling higher contents of BNNT to further enhance the damping behavior. This is in contrast with CNTs which agglomerate at higher concentrations, thus preventing further improvement at higher concentrations. It is observed that for different compositions, tan δ values show no significant changes over varying dynamic loads or prolonged cycles. This shows the ability of nanotube mechanisms to function at varying strain rates and to survive long cycles.

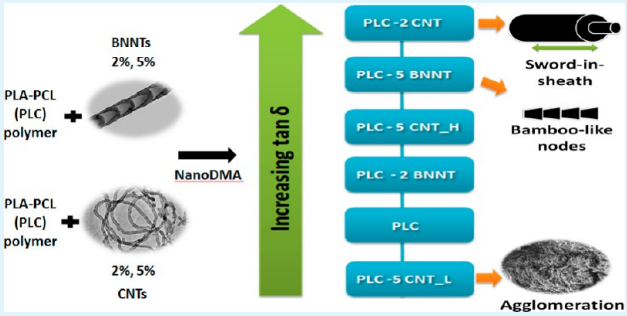

KEYWORDS: *nano dynamic mechanical analysis (nanoDMA), damping, carbon nanotube, boron nitride nanotube, tan delta*

1.0. INTRODUCTION

Boron nitride nanotubes (BNNTs) and carbon nanotubes (CNTs) have greatly attracted the scientific community because of their unique one-dimensional (1D) structure, physical, chemical, and mechanical properties. Structurally, BNNTs are similar to their carbon counterparts. They consist of repeating hexagonal networks of sp^2 hybridized B−N bonds rolled up in a honeycomb lattice[1] while CNTs are repeating sp^2 hybridized carbon bonds. Both have extraordinary thermal and mechanical properties such as comparable Young's moduli of 1.2−1.3 TPa[2,3] and comparable thermal conductivities at room temperature.[4] One major difference between these nanotubes is that BNNTs are chemically stable in air up to ∼1200 K while CNTs are chemically stable only up to ∼750 K.[5] This allows for a wider processing window for synthesizing BNNT reinforced composite materials. The relative chemical inertness of BNNTs at lower temperatures also makes them promising for reinforcing biomaterials.[6,7] As opposed to CNTs which are metallic, semimetallic, or semiconducting depending upon chirality,[8,9] BNNTs are insulating materials with a band gap of 5−6 eV almost independent of tube diameter and chirality.[10] These properties make both types of nanotubes suitable for a variety of applications such as optoelectronic devices,[11] oscillators,[12] and reinforcing structural materials.[13,14] BNNT and CNT based 1D structures have been investigated as reinforcement for developing a variety of composite materials, coatings, and gels.[6,7,13−20]

One important mechanical property for structural applications such as composites is damping behavior since failure in engineering materials typically occurs from accumulated damage. Damping is the dissipation of energy within a material and is of prime importance in dynamic systems such as tracking and pointing weapon systems in aircraft and suspension and steering in automotive and turbo-machinery mountings, which need damping from shock vibrations. Even sports equipment such as golf clubs and tennis racquets require damping to absorb shock waves and alleviate stresses. Fatigue and mechanical loadings are also borne by prosthetics and scaffolds for biomedical applications. Hence improving damping characteristics becomes imperative for enhancing their robustness thereby expanding their lifetimes. Given the importance of damping in biomedical and other applications, here we present a study comparing nanoscale damping characteristics of PLC, a biodegradable copolymer of PLA-PCL (Poly-Lactic Acid and Poly-ϵ-caprolactone), reinforced with BNNTs and CNTs.

In our previous work PLC was reinforced with 2 wt % and 5 wt % BNNTs[6] and 2 wt % and 5 wt % CNTs[15] to study the effect on the mechanical properties and biocompatibility as scaffold material. Both nanotubes improved the mechanical properties of the polymer. The PLC-BNNT composite with 5% BNNT, showed an improvement of 109% and 1370% in tensile

Received: September 9, 2013
Accepted: October 28, 2013
Published: October 29, 2013

strength and elastic modulus respectively as compared to the starting polymer.[6] On the other hand, 2 wt % CNT addition to the virgin PLC enhanced its tensile strength and elastic modulus by 160% and 100% respectively.[15] There was no negative effect on biocompatibility of PLC upon BNNT and CNT addition.[6,15] Here we compare the damping characteristics of our previously synthesized PLC-BNNT and PLC−CNT composites. The damping behavior (tan δ) is characterized through nanodynamical mechanical testing using varying dynamic loads, frequencies, and cycle times. A comparison of the damping behavior of CNT and BNNT is made based on their morphology and dispersion in the PLC matrix.

2.0. MATERIALS AND METHODS

2.1. Materials. The starting copolymer of L-lactide and ε-caproactone (PLC) in 70:30 molar ratio was received from Purac Biomaterials, Lincoln, Illinois. The PLC films were prepared by mixing 1 g of PLC with 20 mL of acetone. The mixture was stirred at 40 °C in a 55 mm beaker using a magnetic stirrer for 20 min. The PLC solution was then cured for 24 h at room temperature in vacuum. The multiwall CNTs and BNNTs were purchased from Nanoamor, Houston, TX. The CNTs had an outer diameter of 40−70 nm and a length of 1−5 μm.[15] The BNNTs had an outer diameter of 32−145 nm and a length of 15−84 μm. Both nanotubes had a purity level of 99%. X-ray diffraction (XRD) analysis in our previous work[6] verified that there were no major impurities in the starting BNNT powder. To prepare the composites, either BNNT or CNT were dispersed in 20 mL of acetone and ultrasonicated for 60 min. The BNNT or CNT mixture was then mixed with the 20 mL PLC-acetone solution and ultrasonicated for another 15 min. The solution was then cured at the same conditions as the pure PLC. The compositions of the films made were pure PLC, PLC-2 wt % BNNT, PLC-5 wt % BNNT, PLC-2 wt % CNT, and PLC-5 wt % CNT. The composites are henceforth referred to as PLC-2BNNT, PLC-5BNNT, PLC-2CNT, and PLC-5CNT. Further details of PLC-BNNT and PLC-CNT composite preparation can be found in our previous studies.[6,15] The composition of 2 and 5 wt % were selected based on literature in the field of nanotube reinforced composites. It has been observed that severe agglomeration of nanotubes occurs at composition greater than 5 wt % whereas excellent dispersion and properties are obtained up to 2 wt %.[20] Hence, 2 wt % (excellent dispersion regime) and 5 wt % (intermediate dispersion regime) were selected to synthesize PLC-nanotube composites.

2.2. Microstructural Characterization. The PLC and PLC-nanotube composites film densities were calculated through geometric measurements. A Philips transmission electron microscope (TEM, model CM 200, Eindhoven, The Netherlands) was used to characterize the starting BNNTs and CNTs. A JEOL JSM-6330F field emission scanning electron microscope (SEM) was used to characterize starting BNNT and CNT powders and the PLC based composite films. The starting powders were characterized using a 15 kV accelerating voltage whereas composite films were characterized using a lower accelerating voltage of 5 kV to avoid damage to the polymer matrix.

2.3. Nanodynamic Mechanical Analysis (NanoDMA). Nanodynamic mechanical analysis (NanoDMA) was performed to characterize the nanoscale damping behavior of the PLC-BNNT and PLC−CNT composites. Hysitron Triboindenter TI900 (Hysitron Inc., Minneapolis, MN, U.S.A.) with a 1 μm conospherical tip was used to perform the NanoDMA tests. The tip-area calibration was done using a standard fused quartz substrate of known modulus (69.6 GPa). NanoDMA experiments consist of a quasistatic loading and a low frequency (<200 Hz) dynamic loading. The damping behavior of viscoelastic materials is characterized by measuring the phase lag δ between the applied forced and the displacement response. This lag is the result of time needed for relaxations in the structure of viscoelastic materials to occur. A perfectly elastic material would have a phase lag of zero. The angle δ allows characterizing the moduli of a material as a complex modulus (E^*), defined in eq 1.

$$E^* = \frac{\sigma}{\varepsilon}(\cos\delta + i\sin\delta) \tag{1}$$

The moduli measured can thus be separated into two distinct moduli, the real part (E') and an imaginary part (E'') as shown in eqs 1−2.

$$E' = \frac{\sigma}{\varepsilon}(\cos\delta) \tag{2}$$

$$E'' = \frac{\sigma}{\varepsilon}(\sin\delta) \tag{3}$$

The real part is the storage modulus (E'), which represents the ability of the material to store potential energy and release it during deformation. The imaginary part is the loss modulus (E'') which represents the viscoelastic component responsible for the dissipated energy. Damping behavior is commonly quantified by the ratio of the loss modulus to the storage modulus which yields tan δ as shown in eq 4.

$$\frac{E''}{E'} = \frac{\left(\frac{\sigma}{\varepsilon}(\sin\delta)\right)}{\left(\frac{\sigma}{\varepsilon}(\cos\delta)\right)} = \tan\delta \tag{4}$$

Higher values of tan δ indicate a higher ratio of viscoelastic to elastic response in the material and, thus tan δ serves as a measure of damping.

In this study, tan δ is evaluated at varying frequencies, varying dynamic loads, and for extended cycles. Figure 1 schematically shows the different types of tests done. Figure 1a shows a frequency sweep load function. During a frequency sweep, the static load and dynamic loadings are held constant, however the frequency increases after each test. In our tests 30 different frequencies in the range 10 to 200 Hz were used. At each frequency, 100 cycles were performed giving a total of 3000 cycles during one frequency sweep. For each sample, frequency sweeps were done at varying dynamic loads. Figure 1b

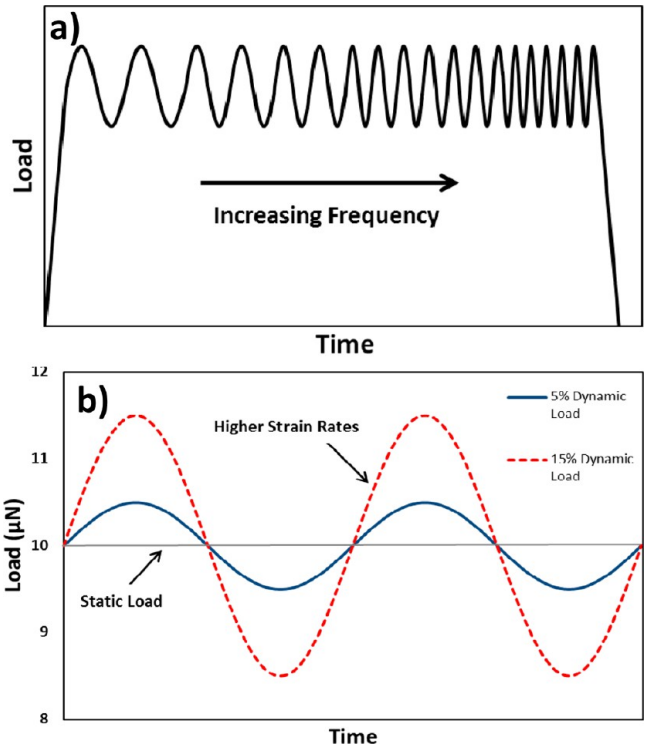

Figure 1. (a) Frequency sweep load function, and (b) varying dynamic load functions.

shows how the loading cycles change as the dynamic load increases. It can be seen that an increase in dynamic load results in higher strain rates and hence more severe loading conditions. The dynamic loads were varied from 5% to 15% of the static load. The static load was 10 μN, so for the 5% dynamic load an oscillating load of 0.5 μN was superimposed. For the 15% dynamic load, a 1.5 μN dynamic load would be applied instead. The last sets of tests were done at 5% dynamic loading at a frequency of 100 Hz, but for a large number (10000, 25000, and 50000) of cycles. These tests enable the evaluation of damping stability at large number of cycles. Constant tan δ values at large number cycles of would indicate damping properties are intact and material is not yet experiencing accumulated damage due to fatigue.

3.0. RESULTS

3.1. Morphology of the Nanotube and PLC-Nanotube Composites. The structure of the CNTs and BNNTs used as reinforcement is shown in the TEM micrographs in Figure 2.

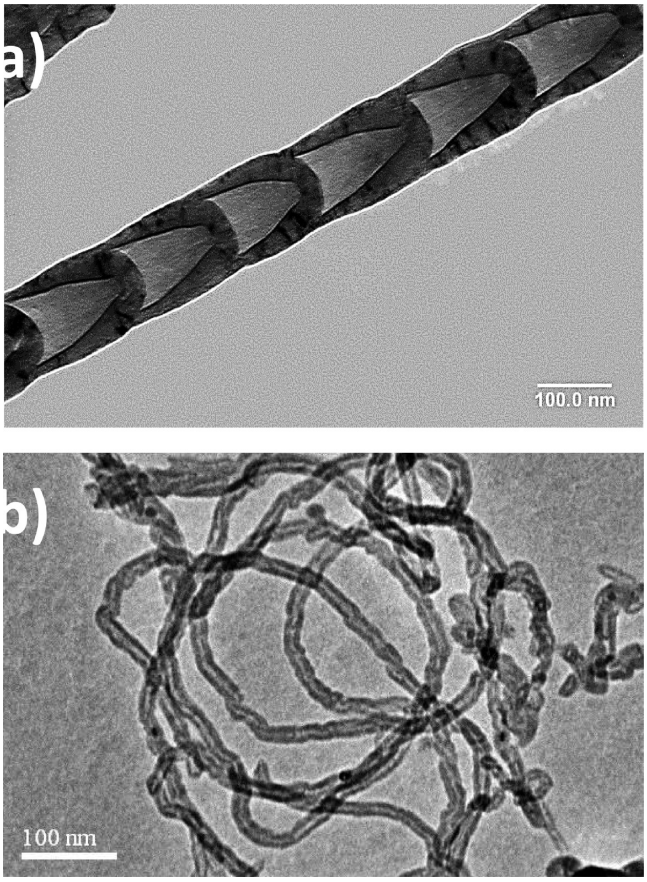

Figure 2. TEM images of (a) starting BNNTs and (b) CNTs. BNNTs exhibit the presence of "bamboo-like" nodes whereas CNTs are tubular with waviness.

Figure 2a shows the nodes in BNNT that give it a "Bamboo-like" structure, which is formed usually as a result of catalytic growth mechanism.[21] This is in sharp contrast to the continuous and wavy tubular structure of the CNT shown in Figure 2b. BNNT used in this study has a significantly larger diameter (32−145 nm) as compared to CNT. The densities of PLC, PLC-2CNT, PLC-5CNT, PLC-2BNNT, and PLC-5BNNT are 0.71, 0.90, 0.69, 1.15, and 1.33 g/cm^3 respectively.[6,15] The discrepancy in densities of PLC-2CNT and PLC-5CNT is a direct consequence of nanotube dispersion in the polymer. CNTs in PLC-2CNT disperse uniformly and conform better to the PLC, leading to higher density. The high content of CNTs in PLC-5CNT induces regions with severe agglomeration and nonuniform nanotube dispersion resulting in higher porosity, which will be discussed later in Figure 6.

3.2. Tan δ Comparison. Figure 3 shows tan δ values at varying frequencies and at different dynamic loads (5% and

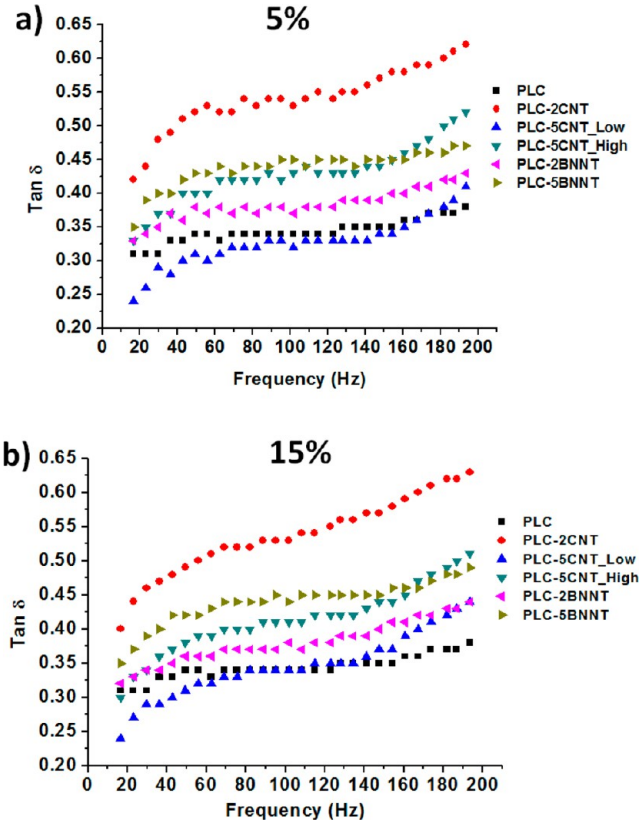

Figure 3. Tan δ variation for different PLC-CNT and PLC-BNNT composites at (a) 5% and (b) 15% dynamic load.

15%). It can be seen in Figure 3a that tan δ is substantially higher (0.4−0.62) for the PLC-2CNT sample at all frequencies. Figure 3b shows that the same result is also observed at the higher dynamic loading of 15%. PLC-5CNT displays a bimodal distribution and is denoted as PLC-5CNT_H for the higher range (0.3−0.51) and PLC-5CNT_L for the lower range (0.24−0.41). Tan δ values decrease as PLC-2CNT, PLC-5BNNT, PLC-5CNT_H, PLC-2BNNT, PLC, and PLC-5CNT_L, in that order, as represented in Figure 4. It is observed that tan δ variation for all the samples is within the range of 0.2−0.65 for both 5% and 15% dynamic loads. The tan δ value increases with the increasing frequency for both varying frequencies and varying dynamic loadings. The damping capacity is retained in 5−15% range of dynamic loading.

The effectiveness of the CNT and BNNT reinforcement on stability of tan δ (damping) is also evaluated at a large number cycles at a constant frequency of 100 Hz. It can be seen from Figure 5 that the damping behavior of all the samples remains fairly constant even when the number of cycles is increased from 10000 to 50000. This indicates that the reinforcing effect and damping mechanisms of both CNTs and BNNTs are not degraded during extended cycle times of up to 50000 cycles. The ability of CNTs and BNNTs to keep dissipating energy in the PLC composite is critical for being an effective damping

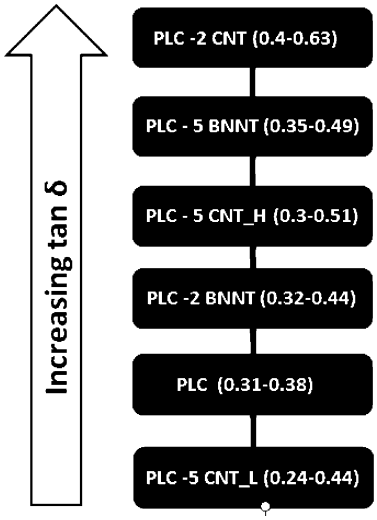

Figure 4. Tan δ of PLC-CNT and PLC-BNNT composites arranged in the increasing order. The values in parentheses are the tan δ values for 15% dynamic load.

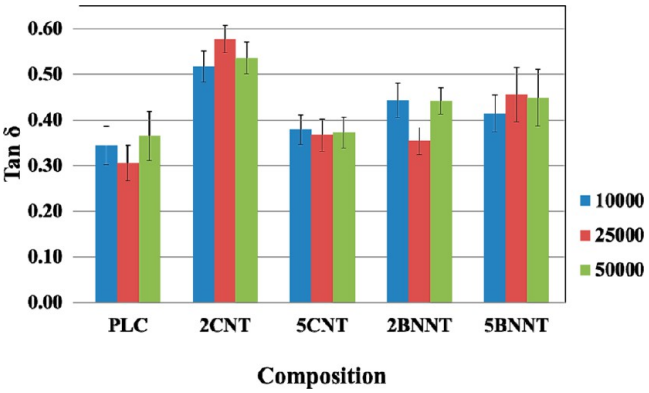

Figure 5. Tan δ comparison for different PLC-CNT and PLC-BNNT composites at 10000, 25000, and 50000 cycles for a frequency of 100 Hz.

material subjected to dynamic loading for large numbers of cycles.

4.0. DISCUSSION

The tan δ results in Figure 3 show that the energy dissipation is most pronounced in PLC-2CNT, followed by other composites with decreasing tan δ as shown in Figure 4. Since both CNTs and BNNTs are tubular structures, energy dissipation can occur via deformation in axial and radial directions. Previous works have reported that BNNTs are radially less rigid than CNTs despite having comparable axial rigidity.[22,23] However, the reported diameters of the nanotubes used in these studies were much lower (1−4 nm) than the nanotubes used in this work. The average diameter of BNNTs used in this work is 71 nm, ranging between 32 and 145 nm. Chiu et al.[24] showed that nanotube morphology plays a key role in determining the radial rigidity of BNNTs. The radial modulus decreases nonlinearly with external radius until it reaches the value of transverse E for hexagonal-boron nitride (h-BN). And thus, the robustness of BNNTs reported in this work, in contrast to previous works[22,23] can be ascribed to their wider diameter. Another reason for stiffer BNNTs can be lack of "sword-in-sheath" mechanism. Sword-in-sheath, also known as telescopic sliding and "stick−slip" also known as pullout, are two well-known mechanisms for energy dissipation within nanotube composites. As validated from the TEM picture (Figure 2a) of the BNNTs used for this study, the presence of "bamboo-like" knots makes the sword-in-sheath motion in BNNTs more difficult as compared to CNTs. As a result of this constricted sliding movement, BNNTs dissipate less energy.

Energy dissipation can also occur via axial deformation of nanotubes in the form of stretching or pullout from the matrix. To compare pullout behavior of BNNT and CNT from the polymer matrix, we have used the interfacial shear strength model proposed by Chen et al.[25] for CNT reinforcement. Since BNNT is a structural analogue of CNT, the model can also be extended to BNNTs as shown by Lahiri et al.[7] for BNNT-hydroxyapatite composite.[7] The effective area of outer layers (A_{eff}) carrying the load in a multiwall nanotube is calculated as follows

$$A_{eff} = \pi \sum_{m=1}^{N} \{[R_{NT} - (m-1)h - (m-1)h']^2 - [R_{NT} - mh - (m-1)h']^2\} \quad (5)$$

where, R_{NT} refers to the outer radius of the respective nanotube (the average outer radius for BNNT is ∼35.5 nm and ∼25 nm for CNT), h is the effective layer thickness (∼0.25 nm for BNNT[26] and ∼0.075 nm for CNT [27]) $h' = h - d$ where d is the spacing between each graphene/h-BN layer (∼0.34 nm for CNT[27] and ∼0.33 nm for BNNT[28]) and N is the number of outer layers carrying the load. For a conservative estimate, it is assumed that load is borne by the outer 5 walls for both the nanotubes. To calculate the interfacial shear strength (ζ) between the nanotubes and a polymer matrix, the Cox model is used.

$$\zeta = \frac{E_{NT} \times e \times A_{eff} \times \beta}{2\pi R_{CNT}} \times \frac{\sinh \beta\left(\frac{L}{2} - x\right)}{\cosh \frac{\beta L}{2}} \quad (6)$$

where

$$\beta = \sqrt{\left(\frac{G'_{Polymer}}{E_{NT}}\right)\left(\frac{2\pi}{A_{eff} \ln R/R_{NT}}\right)} \quad (7)$$

R is the radius of the polymer matrix cylinder, e is the applied strain, L is the average length of the nanotube (∼1.98 μm for BNNT and ∼2 μm for CNT), x is the distance from the end of the nanotube. $G'_{Polymer}$ is the shear modulus of the polymer in which the nanotubes are embedded, and E_{NT} is the elastic modulus of the respective nanotube (∼750 GPa for BNNT[29], ∼ 800 GPa for CNT[30]). R/R_{NT} is estimated using the following equation:

$$\left(\frac{R}{R_{NT}}\right)^2 = \frac{\pi}{4V_f} \quad (8)$$

V_f is the volume fraction of the respective nanotube in the polymer matrix. We have calculated shear stress values for 2 wt % compositions for both the nanotubes (∼ 0.0124 for BNNT and ∼0.0158 for CNT). Table 1 lists the ratio of shear stress calculated for BNNT and CNT for ethylene based and poly lactide polymer matrixes. The shear stress ratio for PLC could not be computed because the shear modulus value for PCL is not available in the literature.

Table 1. Ratio of BNNT and CNT Shear Stress in the Respective Polymer Matrix

polymer	$G'_{polymer}$ (GPa)	ζ_{BNNT}/ζ_{CNT}
HDPE	0.85[31]	1.44
MDPE	0.66[31]	1.43
LDPE	0.16[31]	1.31
PLA	1.24[32]	1.44

It can be seen that $\zeta_{BNNT}/\zeta_{CNT} > 1$, implying that the force required to pullout BNNT from the polymer matrix is much higher than that required for CNT, making pullout easier in CNTs as compared to BNNTs. This facile pullout along with easier sword-in-sheath makes CNTs more prone to deformation, leading to more energy dissipation in CNTs and therefore, resulting in a higher tan δ and damping.

It was seen in Figures 3 and 4 that PLC-5CNT had a bimodal distribution of tan δ values. The different sets of values of tan δ result from "good" and "bad" regions in the composite. Good regions are where CNTs are well dispersed in the polymer while bad regions are where CNTs tend to agglomerate. The varying microstructures of these regions are shown in Figure 6. As can be seen from the Figure 6c, CNTs

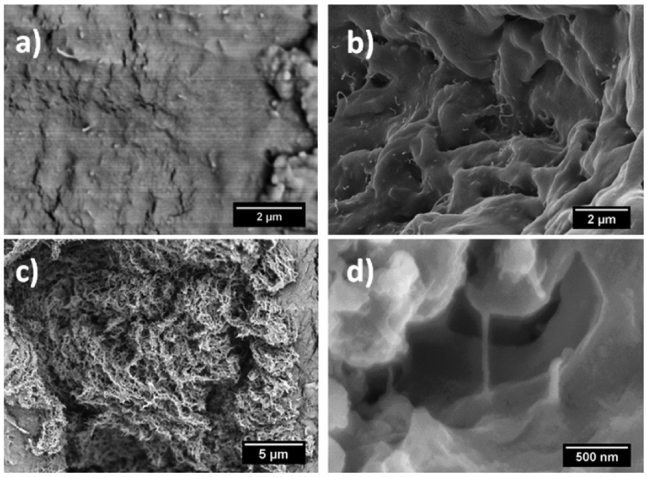

Figure 6. (a) PLC-2CNT shows uniform dispersion of nanotubes within the polymer while PLC-5CNT composite shows regions of (b) good and (c) bad dispersion. CNTs are well dispersed within the polymer matrix in (b) while in (c) CNTs are agglomerated. This nonuniformity in dispersion leads to bimodal distribution in damping. (d) PLC-5BNNT sample showing the "bridging" mechanism between the polymer and BNNTs.

are not well-dispersed and tend to agglomerate when present in larger amounts (5 wt %). On the other hand it can be seen from Figure 6d that BNNTs in the 5 wt % composite tend to conform to the polymer matrix much better owing to the formation of "bridge-like" structures between the PLC and BNNTs. Better dispersion of BNNTs in the polymer can be ascribed to the electric polarization induced in BNNTs along the axis as a result of broken 3-fold symmetry.[33] This electric polarization helps the BNNT adhere to the polymer better, preventing agglomeration and resulting in better dispersion and hence in better damping with increasing concentration.

It is also seen in Figure 5 that tan δ values for the composites along with that of PLC show almost imperceptible changes over cycles in the range of 10000−50000. This shows that nanotube mechanisms leading to damping can sustain for prolonged cycles. One of the major damage mechanisms during cyclic loading is the formation of microcracks that propagate along the process and become unstable after exceeding a critical threshold. This culminates in fast fracture and the failure of the composite. Grimmer et al.[34] proposed that CNTs hinder the formation of large cracks by nucleating nanoscale damage zones. The addition of CNTs decreases the scale of damage mechanisms; thereby increasing the absorption of strain energy. Zhang et al.[35] demonstrated that CNTs suppress failure through crack-bridging and frictional pullout. These mechanisms enhance the long-term behavior of composites under cyclic loading, which is evident from our tan δ results. And since damping is the measure of energy dissipation, the addition of CNTs will prevent failure through energy release in the form of crack-bridging and pullout, thereby improving the damping characteristics.

5.0. CONCLUSIONS

The damping behavior of CNT and BNNT reinforced PLC was investigated by nanodynamic mechanical analysis to evaluate which nanotube filler leads to superior damping enhancement. Among all the compositions, 2 wt % CNTs showed the highest enhancement in damping behavior. The superior damping with CNT reinforcement as compared to BNNT reinforcement is attributed to "sword-in-sheath" and "lower interfacial shear strength" phenomenon of CNT. The effectiveness of "sword-in-sheath" mechanism is compromised in BNNTs because of their discontinuous bamboo-like structure. Cox model estimations show that CNTs have lower shear strength in the polymer matrix, leading to easier pullout and higher energy dissipation. CNTs show poorer damping behavior with increasing concentration (5 wt %) because of agglomeration. In contrast, BNNTs show superior damping when present in larger (5 wt %) amounts. This is a result of the better dispersion of BNNTs in the PLC matrix. It is expected that increase in CNT content would also lead to improvement in damping behavior if the CNTs could be more effectively dispersed in the PLC matrix. The damping behavior (tan δ) is not affected up to 50000 loading cycles indicating energy dissipation mechanisms are effective and do not die down due to fatigue.

AUTHOR INFORMATION

Corresponding Author

*E-mail: agarwala@fiu.edu.

Notes

The authors declare no competing financial interest.

ACKNOWLEDGMENTS

R.A. acknowledges the University Graduate School (UGS) at Florida International University for support through a Presidential Fellowship. The authors acknowledge the support of the Advanced Materials Engineering Research Institute (AMERI) at FIU for providing the characterization facilities.

REFERENCES

(1) Chopra, N. G.; Luyken, R. J.; Cherrey, K.; Crespi, V. H.; Cohen, M. L.; Louie, S. G.; Zettl, A. *Science* **1995**, *269*, 966−967.

(2) Krishnan, A.; Dujardin, E.; Ebbesen, T. W.; Yianilos, P. N.; Treacy, M. M. J. *Phys. Rev. B: Condens. Matter Mater. Phys.* **1998**, *58*, 14013−14019.

(3) Chopra, N. G.; Zettl, A. *Solid State Commun.* **1998**, *105*, 297−300.

(4) Chang, C. W.; Fennimore, A. M.; Afanasiev, A.; Okawa, D.; Ikuno, T.; Garcia, H.; Li, D.; Majumdar, A.; Zettl, A. *Phys. Rev. Lett.* **2006**, *97* (085901), 1−4.
(5) Golberg, D.; Bando, Y.; Kurashima, K.; Sato, T. *Scr. Mater.* **2001**, *44*, 1561−1565.
(6) Lahiri, D.; Rouzaud, F.; Richard, T.; Keshri, A. K.; Bakshi, S. R.; Kos, L.; Agarwal, A. *Acta Biomater.* **2010**, *9*, 3524−33.
(7) Lahiri, D.; Singh, V.; Benaduce, A. P.; Seal, S.; Kos, L.; Agarwal, A. *J. Mech. Behav. Biomed. Mater.* **2011**, *4*, 44−56.
(8) Hamada, N.; Sawada, S.; Oshiyama, A. *Phys. Rev. Lett.* **1992**, *68*, 1579−1581.
(9) Saito, R.; Fujita, M.; Dresselhaus, G.; Dresselhaus, M. S. *Appl. Phys. Lett.* **1992**, *60*, 2204−2206.
(10) Blasé, X.; Rubio, A.; Louie, S. G.; Cohen, M. L. *Euro-Phys. Lett.* **1994**, *28*, 335−340.
(11) Sheng, W.; ZhiYong, Z.; LianMao, P. *Chin. Sci. Bull.* **2012**, *57*, 149−156.
(12) Sazonova, V.; Yaish, Y.; Ustunel, H.; Roundy, D.; Arias, T. A.; McEuen, P. L. *Nature* **2004**, *431*, 284−287.
(13) Bakshi, S. R.; Lahiri, D.; Agarwal, A. *Int. Mater. Rev.* **2010**, *55*, 41−64.
(14) Lahiri, D.; Hadjikhani, A.; Zhang, C.; Xing, T.; Li, L. H.; Chen, Y.; Agarwal, A. *Mater. Sci. Eng., A* **2013**, *574*, 149−156.
(15) Lahiri, D.; Rouzaud, F.; Namin, S.; Keshri, A. K.; Valdés, J. J.; Kos, L.; Tsoukias, N.; Agarwal, A. *ACS App. Mater. Interfaces* **2009**, *11*, 2470−2476.
(16) Zou, J.; Liu, J.; Karakoti, A. S.; Kumar, A.; Joung, D.; Li, Q.; Khondaker, S. I.; Seal, S.; Zhai, L. *ACS Nano* **2010**, *4* (12), 7293−7302.
(17) Balani, K.; Zhang, T.; Karakoti, A.; Li, W.; Seal, S.; Agarwal, A. *Acta Mater.* **2008**, *56* (5), 571−579.
(18) Laha, T.; Liu, Y.; Agarwal, A. *J. Nanosci. Nanotechnol.* **2007**, *7* (2), 515−524.
(19) Balani, K.; Agarwal, A. *Nanotechnology* **2008**, *19*, 165701.
(20) Bakshi, S. R.; Agarwal, A. *Carbon* **2011**, *49* (2), 533−544.
(21) Tang, C. C.; Chapelle Lamy De La, M.; Li, P.; Liu, Y. M.; Dang, H. Y.; Fan, S. S. *Chem. Phys. Lett.* **2001**, 492−496.
(22) Zheng, M.; Zou, L.-F.; Wang, H.; Park, C.; Ke, C. *ACS Nano* **2012**, *6*, 1814−1822.
(23) Zheng, M.; Ke, C.; Bae, I.-T.; Park, C.; Smith, M. W.; Jordan, K. *Nanotechnology* **2012**, *23* (095703), 1−10.
(24) Chiu, H.-C.; Kim, S.; Klinke, C.; Riedo, E. *Appl. Phys. Lett.* **2012**, *101* (103109), 1−5.
(25) Chen, Y.; Balani, K.; Agarwal, A. *Appl. Phys. Lett.* **2008**, *92*, 011916−011918.
(26) Lan, H.; Ye, L.; Zhang, S.; Peng, L. *Appl. Phys. Lett.* **2009**, *94*, 183110−183112.
(27) Lau, K. T. *Chem. Phys. Lett.* **2003**, *370*, 399−405.
(28) Terrones, M.; Romo-Herrera, J. M.; Cruz-Silva, E.; López-Urías, F.; Muñoz-Sandoval, E.; Velázquez-Salazar, J. J.; Terrones, H.; Bando, Y.; Golberg, D. *Mater. Today* **2007**, *10*, 30−38.
(29) Suryavanshi, A. P.; Yu, M. F.; Wen, J.; Tang, C.; Bando, Y. *Appl. Phys. Lett.* **2004**, *84*, 2527−2529.
(30) Demczyk, B. G.; Wang, Y. M.; Cumings, J.; Hetman, M.; Han, W.; Zettl, A.; Ritchie, R. O. *Mater. Sci. Eng., A* **2002**, *334*, 173−178.
(31) Martienssen, W.; Warlimont, H. *Springer Handbook of Condensed Matter and Materials Data*; Springer: Heidelberg, Germany, 2005; Vol. *XVII*, p 484.
(32) Jamshidian, M.; Tehrany, E. A.; Imran, M.; Jacquot, M.; Desobry, S. *Compr. Rev. Food Sci. Food Saf.* **2010**, *9*, 552−571.
(33) Mele, E. J.; Král, P. *Phys. Rev. Lett.* **2002**, *88*, 056803.
(34) Grimmer, C. S.; Dharan, C. K. H. *J. Wuhan Univ. Technol., Mater. Sci. Ed.* **2009**, *24*, 167−173.
(35) Zhang, W.; Picu, R. C.; Koratkar, N. *Appl. Phys. Lett.* **2007**, *91*, 193109.